

# A Minimal Interpretation of the Galactic Cosmic-Ray Spectrum from GeV to PeV Energies

FELIX AHARONIAN<sup>1, 2, 3, 4</sup> AND B. THEODORE ZHANG<sup>5, 3</sup><sup>1</sup>Yerevan State University, 1 Alek Manukyan Street, Yerevan 0025, Armenia<sup>2</sup>University of Science and Technology of China, 230026 Hefei, China<sup>3</sup>TIANFU Cosmic Ray Research Center, 610000 Chengdu, China<sup>4</sup>Max-Planck-Institut for Nuclear Physics, P.O. Box 103980, 69029 Heidelberg, Germany<sup>5</sup>Institute of High Energy Physics, Chinese Academy of Sciences, 100049 Beijing, China

## ABSTRACT

High-precision measurements of the cosmic-ray (CR) proton spectrum have revealed significant deviations from a simple power-law behaviour. These deviations are characterised by three prominent features: (i) a progressive spectral hardening above approximately 200 GeV, (ii) an excess between 10 and 30 TeV (the “multi-TeV bump”), followed by a sharp turnover around 100 TeV, and (iii) a pronounced structure between 0.1 and 10 PeV (the “PeV bump”). We propose a minimal two cosmic-ray population framework that consistently accounts for the observed CR proton spectrum across six decades in energy, from GeV to PeV. In this scenario, the spectral complexity arises naturally from a transition between two Galactic CR proton populations in the 10–100 TeV energy range. The low-energy population exhibits a sharp cutoff at tens of TeV, while a second, higher-energy population emerges and dominates above 100 TeV, terminating with a smooth exponential cutoff at approximately 6.5 PeV. This framework reproduces all observed spectral features without invoking contributions from nearby sources or requiring non-standard assumptions about particle acceleration or propagation. Recent gamma-ray observations of supernova remnants, star-forming regions, and microquasars provide plausible astrophysical candidates for the origin of the two CR components.

*Keywords:* cosmic rays — supernova remnants — stellar clusters — microquasars — gamma rays: Galaxy — acceleration of particles

## 1. INTRODUCTION

Until recently, Galactic cosmic-rays (CRs) were generally considered to constitute a single population characterised by a featureless power-law spectrum extending up to the so-called *knee* at energies of a few PeV. The conceptual framework, commonly referred to as the SNR CR paradigm (Ginzburg & Syrovatskii 1964; Berezinskii et al. 1990; Blandford & Eichler 1987; Blasi 2013), attributes the bulk of the Galactic CR flux to particles accelerated in supernova remnants (SNR) via the so-called process of diffusive shock acceleration (DSA; see Malkov & Drury 2001 for a review). In its simplest test-particle formulation, DSA at strong shocks predicts a power-law source spectrum with index  $\Gamma = 2$ .

More realistic, time-dependent treatments that include shock obliquity and deceleration, evolving magnetic turbulence, and energy-dependent particle escape predict steeper source spectra,  $\Gamma \simeq 2.3$ –2.4. Subsequent energy-dependent propagation of CRs in Galactic magnetic fields further steepens the CR energy distribution,

resulting in an observed spectrum close to  $E^{-2.7}$  (Strong et al. 2007; Grenier et al. 2015; Gabici et al. 2019).

Within this framework, the spectral feature known as *knee*, first identified in the late 1950s (Kulikov & Kristiansen 1959) and widely interpreted as marking the termination of the Galactic CR component at the maximum energy achievable in young supernova. However, conservative theoretical treatments show that, under standard conditions, proton energies are unlikely to exceed 100 TeV (Lagage & Cesarsky 1983). This tension has motivated extensions of the standard DSA concept by proposals such as magnetic-field amplification driven by nonlinear CR-induced instabilities (Bell 2004), or by rigidity-dependent interpretations in which the *knee* reflects the cutoff of heavier nuclei, whereas protons terminate at lower energies (Hörandel 2003).

Recent high-precision measurements of the Galactic CR proton spectrum have significantly refined this picture. Data from space- and ground-based experiments, spanning nearly six decades in energy and largely

free from nuclear-composition ambiguities, reveal clear deviations from a simple power-law behaviour. The spectrum exhibits a gradual hardening beginning at  $\sim 200$  GeV, followed by saturation and subsequent softening in the multi-TeV range (see Fig.1), resulting in a relatively narrow spectral feature at several tens of TeV, hereafter referred to as the *multi-TeV bump*.

Although the energy range between several tens and a few hundred TeV is affected by non-negligible statistical and systematic uncertainties, current data indicate a distinct spectral turnover near 100 TeV. At higher energies, measurements extending into the PeV domain reveal an additional broad spectral structure characterized by a pronounced maximum at several PeV, hereafter referred to as the *PeV bump*. Identification of the proton component extending to at least 10 PeV resolves the degeneracy associated with heavy-nuclei contribution and suggests the existence of CR proton PeVatrons.

The presence of multiple distinct spectral structures cannot be adequately explained within the framework of a single CR population scenario. Recent data have prompted alternative interpretations that propose unconventional acceleration mechanisms, revised propagation scenarios, or substantial contributions from nearby astrophysical sources.

In this work, we show that the superposition of two broadband Galactic CR components, characterised by different power-law indices and cutoff energies separated by approximately two orders of magnitude in energy, can naturally reproduce all observed spectral features. This phenomenological approach does not require non-standard acceleration or propagation mechanisms (Blasi et al. 2012), nor does it rely on local effects, such as dominant nearby sources (Liu et al. 2019; Alemanno et al. 2025a), or spectral distortions induced by local shocks (Malkov & Moskalenko 2021).

While earlier experiments such as PAMELA (Adriani et al. 2011) and CREAM (Ahn et al. 2010) provided initial evidence of these spectral features, and complementary measurements from CALET (Adriani et al. 2022), NUCLEON (Atkin et al. 2017), and KASCADE (Antoni et al. 2005), GRAPES (Varsi et al. 2024) contributed valuable data, this analysis focuses exclusively on AMS-02 (Aguilar et al. 2015), DAMPE (Alemanno et al. 2025b), and LHAASO (Cao et al. 2025) datasets selected for their superior precision and broad energy coverage.

## 2. TWO CR POPULATION MODEL

### 2.1. *The framework*

We describe the Galactic CR proton spectrum as the superposition of two distinct components, each charac-

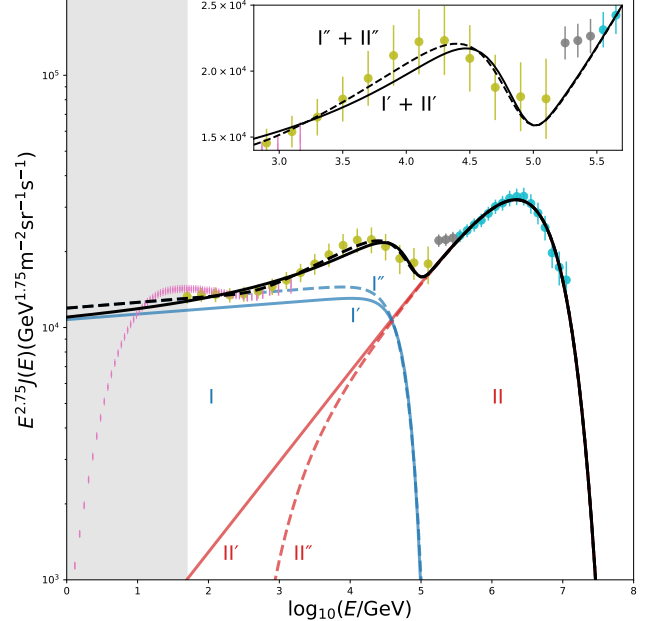


**Figure 1.** CR proton spectrum multiplied by  $E^{2.75}$ , with fit curves compared to measurements from AMS-02 (Aguilar et al. 2015), DAMPE (Alemanno et al. 2025b), and LHAASO (Cao et al. 2025). The blue and red curves represent the contributions of the first (I) and second (II) CR components, respectively. Two alternative assumptions for the extrapolation of the second CR component toward low energies are shown: (a) a pure power-law extrapolation (curves I' and II') and (b) a scenario with low-energy hardening of the second component (curves I'' and II''), as discussed in the text. The solid and dashed black curves show the total proton spectrum in the two-component CR framework for the (a) and (b) scenarios, respectively. The corresponding best-fit parameters are listed in Table 1. The inset highlights the spectral structure in the multi-TeV energy range. The grey shaded region below 50 GeV indicates the energy range strongly affected by solar modulation.

terised by a power-law distribution with a high-energy cutoff. At this stage, the two components are introduced phenomenologically, without specifying their physical origin, in order to provide a minimal description of the observed spectrum over the entire GeV-PeV energy range. We write the total proton flux as

$$J_{\text{tot}}(E) = J_1(E) + J_2(E), \quad (1)$$

where  $J_1(E)$  denotes the low- to intermediate-energy component dominating at GeV and TeV energies, and  $J_2(E)$  represents a second, harder component with a much higher cutoff energy. Both components are parameterised using the same functional form,

$$J_i(E) = A_i E^{-\Gamma_i} \exp \left[ - \left( \frac{E}{E_{i,0}} \right)^{\beta_i} \right], \quad (2)$$

where  $A_i$  is the normalisation,  $\Gamma_i$  the power-law spectral index,  $E_{i,0}$  the characteristic cutoff energy, and the parameter  $\beta_i$  controls the sharpness of the cutoff for  $i = 1$  and  $i = 2$  components. The adopted functional form is not intended to offer a description of acceleration or transport processes, but rather to extract the characteristic energy scales, spectral slopes, and cutoff energies that are directly implied by the observations. It is sufficiently general to provide a flexible phenomenological description applicable to a broad range of astrophysical scenarios.

Typically, the superposition of two broad spectral components, such as two power-law functions with different slopes, results in a smooth, gradual transition in the total spectrum near the energy at which their contributions become comparable. However, the measured CR proton spectrum does not exhibit this expected behavior. Instead, the data reveal a relatively weak but noticeable excess in the multi-TeV range, followed by a pronounced and sharp turnover within a narrow energy interval around approximately 100 TeV (see Fig. 1).

To accurately reproduce the observed turnover within such a narrow energy interval, the low-energy component must be sharply suppressed above its characteristic cutoff energy. In practice, this requires a cutoff significantly steeper than a simple exponential, for example, a super-exponential form with  $\beta_1 > 1$  in Eq. (2). As a result, the contribution of the first component becomes strongly suppressed at energies above  $\sim 100$  TeV.

At higher energies, the observed spectrum is dominated by the second component, which allows its spectral shape to be constrained directly by measurements in the PeV range, where the influence of the first component is minimal. Once the high-energy component is determined in this regime, its contribution can be extrapolated toward lower energies. Subtracting this extrapolated contribution from the measured CR proton flux then yields the spectrum of the low-energy component.

## 2.2. Results

Using the two-component framework described above, we fit the measured proton spectrum from 100 GeV to 10 PeV. At the highest energies, above  $\sim 300$  TeV, the observed spectrum is strongly dominated by the second component, allowing its spectral parameters to be constrained exclusively by the LHAASO measurements. In this energy range, the high-energy component is well described by a power-law spectrum with index  $\Gamma_2 \simeq 2.4$

and an exponential cutoff ( $\beta_2 = 1$ ) at  $E_{2,0} \simeq 6.2$  PeV (see Table 1)<sup>1</sup>.

Extrapolating this component to lower energies and subsequently subtracting it from the measured data yields the first proton component. It is defined by a spectral index  $\Gamma_1 \simeq 2.7$ , a cutoff energy  $E_{1,0} \simeq 67.6$  TeV, and a super-exponential cutoff parameterized by  $\beta_1 \simeq 2.5$  (see Table 1). The resulting superposition of the two components' spectra reproduces the observed multi-TeV bump, the sharp turnover near 100 TeV, and the broad spectral structure in the PeV range.

The fit parameters presented in Table 1 were derived from a joint analysis of the DAMPE and LHAASO data sets. The AMS-02 data were excluded from the fitting procedure because they exhibit excellent agreement with the DAMPE measurements in the overlapping energy range.

We note a modest deviation in the LHAASO data below  $\sim 300$  TeV range. These points suggest an unusually flat local spectral behavior that is difficult to reconcile with the current model and with general expectations from diffusive acceleration and propagation scenarios. In principle, this behavior could be reproduced by the presence of an additional, narrowly confined spectral component. However, the deviation in absolute flux does not exceed 10%, and, more importantly, this energy interval is close to the LHAASO detection threshold, where systematic uncertainties associated with energy reconstruction and detector response are expected to be significant. For these reasons, an independent fit to these points is not attempted at this stage. Instead, the analysis focuses on the global spectral behavior, which is robustly described by the two-component framework. If future measurements confirm the presence of such a feature confined to the narrow energy interval between approximately 100 and 300 TeV, its interpretation within the current framework or within any standard cosmic-ray acceleration and propagation model would be highly challenging.

The extrapolation of the high-energy component to GeV energies is not uniquely constrained by the available data. Although a power-law extrapolation is permitted within standard acceleration or propagation models, alternative low-energy behaviors remain plausible. As an illustrative test, a variant is considered in which the second component exhibits low-energy hard-

<sup>1</sup> To avoid implying unrealistically high accuracy, the parameter values in the text are rounded, whereas Table 1 presents the formal best-fit values obtained from the fitting procedure.

**Table 1.** Fit parameters for the two-component CR proton model

Model	$A$ ( $\text{GeV}^{1.75} \text{ m}^{-2} \text{ s}^{-1} \text{ sr}^{-1}$ )	$\Gamma$	$E_0$ (TeV)	$\beta$	$E_{\min}$ (TeV)
First component					
I'	$14500^{+2500}_{-1900}$	$2.73 \pm 0.02$	$68^{+18}_{-14}$	$2.55^{+1.32}_{-0.90}$	...
I''	$16200^{+4200}_{-2700}$	$2.73^{+0.02}_{-0.03}$	$63^{+16}_{-12}$	$2.18^{+1.31}_{-0.74}$	...
Second component					
II'	$34700 \pm 1600$	$2.39 \pm 0.05$	$6200^{+900}_{-800}$	1 (fixed)	...
II''	34700 (fixed)	2.39 (fixed)	6200 (fixed)	1 (fixed)	$0.89^{+1.30}_{-0.57}$

The fitting function  $E^{2.75}J(E)$  is presented in the form

$$E^{2.75}J(E) = A \left( \frac{E}{E^*} \right)^{2.75-\Gamma} \exp \left[ - \left( \frac{E}{E_0} \right)^\beta \right] \exp \left[ \left( -\frac{E_{\min}}{E} \right) \right],$$

where  $E_0$ ,  $\Gamma$ , and  $\beta$  are the fit parameters listed in the table,  $E^* = 10^3$  TeV is a fixed pivot energy. The normalization parameter  $A$  is given in units of  $\text{GeV}^{1.75} \text{ m}^{-2} \text{ s}^{-1} \text{ sr}^{-1}$ , corresponding to the representation shown in Fig.1. The first CR component is obtained from a joint fit to the DAMPE and LHAASO data, while the second component is constrained exclusively using LHAASO data above  $E > 300$  TeV.

ening, as indicated by the curve labeled II' in Fig.1. Specifically, it is assumed that below the TeV scale, the spectrum deviates from a pure power-law extrapolation due to an additional suppression term proposed in the form  $\exp[-E_{\min}/E]$ , with  $E_{\min} \simeq 0.9$  TeV.

In this scenario, a slight modification to the normalization of the first proton component continues to provide an accurate representation of the data, resulting in only minor changes in the fitted parameters (see Table 1). This result demonstrates the robustness of the two-component interpretation when subjected to variations in the low-energy behavior of the second proton component within reasonable limits. Otherwise, i.e., a sharper cutoff of the second proton component below TeV energies, would preclude the first proton component spectrum from maintaining a power-law form with a fixed, energy-independent index to account for the gradual hardening observed in the measured proton spectrum above 200 GeV.

The parameter values listed in Table 1 should be considered as representative examples rather than unique solutions. They illustrate the minimal constraints imposed by the observational data. Nevertheless, these parameters cannot deviate arbitrarily from the values in Table 1 without degrading the fit quality. Specifically, both the power-law index and the sharp cutoff of the first component below approximately 100 TeV are tightly constrained by observations. The parameters of the second component are well constrained at PeV en-

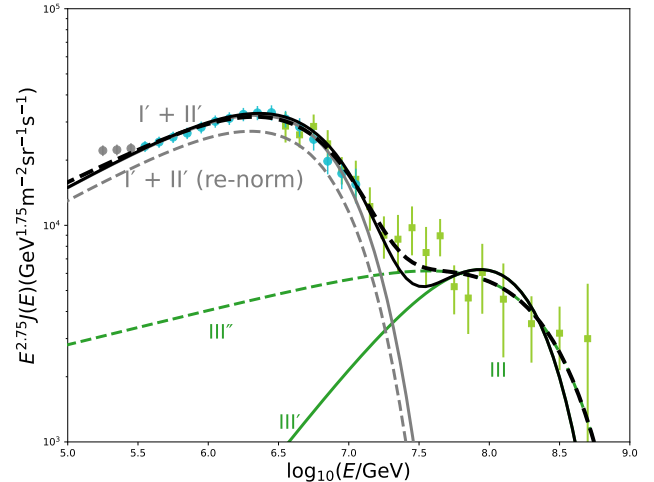


**Figure 2.** CR proton spectrum multiplied by  $E^{2.75}$ , with fit curves compared to the LHAASO (Cao et al. 2025) and IceTop(Aartsen et al. 2019) measurements. The grey and green curves represent the contributions of the second (II') and the third (III') proton components, respectively. The sum of the second and third components is shown by the black curves. The solid curves correspond to the case when the flux of I' + II' is fixed and coincides with the flux in Fig.1 for the scenario (a). The dashed curves are obtained from the joint LHAASO and IceTop data fit. The corresponding best-fit parameters are listed in Table 2.

ergies, with the main remaining uncertainty related to its extrapolation to lower energies.

**Table 2.** Fit parameters for the third CR proton component

Model	$A$ ( $\text{GeV}^{1.75} \text{m}^{-2} \text{s}^{-1} \text{sr}^{-1}$ )	$\Gamma_3$	$E_{\text{max}}$ PeV
Third component <sup>a</sup>			
Fixed II'	$340^{+280}_{-170}$	$1.91^{+0.19}_{-0.21}$	$102^{+43}_{-26}$
Third component <sup>b</sup>			
Free II'	$4100 \pm 2000$	$2.59^{+0.12}_{-0.19}$	$229^{+178}_{-85}$

<sup>a</sup>Third component is fitted assuming the second component is fixed to its best-fit parameters (II').

<sup>b</sup>Third component is obtained from a joint fit in which the normalisation and cutoff energy of the second component are allowed to vary, while its spectral index is fixed at  $\Gamma_2 = 2.4$ . This yields  $E_{2,0} = 5.6^{+0.3}_{-0.4}$  PeV and  $A_2 = (3.02 \pm 0.28) \times 10^4$   $\text{GeV}^{1.75} \text{m}^{-2} \text{s}^{-1} \text{sr}^{-1}$  for the second component.

The detailed shape of the spectrum in the multi-PeV range may, however, be influenced by an additional contribution from a third CR proton component at energies of several tens to hundreds of PeV. As shown in Fig.2, the fluxes reported by the IceTop collaboration (Aartsen et al. 2019) in this energy range lie significantly above the extrapolation of the two-component spectrum, suggesting the emergence of a new CR proton population. Its origin may be Galactic or extragalactic, but this distinction is not essential for the purposes of this paper.

To investigate the interplay between the second and third proton components, we performed a joint fit to the combined LHAASO and IceTop data from 0.3 to  $\simeq 500$  PeV. As a first step, we assumed that the contribution of the third proton component below 10 PeV is negligible, such that the combined spectrum of the first and second components remains unchanged. In practice, this corresponds to fixing the second component since the contribution of the first component in this energy band is negligible. Specifically, in the fitting procedure, we fix the second component to II', corresponding to scenario (a) in Fig.1. Under this assumption, the resulting third component is characterised by a very hard power-law spectrum with  $\Gamma_3 \simeq 1.9$  and an exponential cutoff at  $E_{0,3} \simeq 100$  PeV (see Fig.2 and Table 2).

The agreement of this model with the data in the transition region around  $\sim 30$  PeV is only marginal. The fit is improved when allowing the parameters of the second component to vary together with the third component. Although the measurements in this energy interval are affected by large statistical uncertainties, they favour a

softer proton spectrum with  $\Gamma_3 \gtrsim 2.6$  and a much higher cutoff energy.

In this joint-fit procedure, the parameters of the second component change only modestly: its normalisation is slightly reduced, and its cutoff energy decreases to  $E_{2,0} \simeq 5.8$  PeV, compared to  $\simeq 6.3$  PeV in the pure two-component fit (see Fig.2 and Table 2). This spectral stability is readily understood. In the representation  $E^{2.75} J(E)$ , the flux at tens of PeV is substantially lower than that at a few PeV, implying that the third component cannot have a strong impact on the derived spectrum in the PeV range. While, in principle, the contribution of the third component below  $\sim 10$  PeV could be increased by assuming an even steeper spectrum, such a scenario would contradict the IceTop measurements at the highest energies. We therefore conclude that the spectrum of the second component inferred from the LHAASO data is stable and largely unaffected by the presence of the third CR component.

In Fig.3, we present the posterior probability distributions for the spectral parameters of the second CR proton component. The results show that both the spectral index,  $\Gamma_2$ , and the characteristic cutoff energy,  $E_{2,0}$ , are confined to remarkably narrow ranges, even when the sharpness of the cutoff,  $\beta_2$ , is treated as a free parameter. The best-fit values are  $\Gamma_2 = 2.36^{+0.12}_{-0.17}$ ,  $E_{2,0} = 6.7^{+0.17}_{-0.37}$  PeV, and  $\beta_2 = 0.91^{+0.38}_{-0.29}$  (see Table 2), demonstrating that the PeV-scale cutoff of the second component is robustly determined by the LHAASAO data.

In summary, the Galactic CR proton spectrum from GeV to PeV energies can be well described by the superposition of two broad components with power-law indices  $\Gamma_1 \simeq 2.7$  and  $\Gamma_2 \simeq 2.4$ , extending effectively up to  $\sim 65$  TeV and  $\sim 6.5$  PeV, respectively. The first component terminates sharply, requiring a super-exponential cutoff with  $\beta_1 \geq 2$ , whereas the second CR component is well described by a simple exponential cutoff. Their overlap near  $\sim 100$  TeV naturally produces the observed multi-TeV bump, followed by a sharp spectral turnover, in good agreement with the data. Within this framework, the gradual hardening of the spectrum from hundreds of GeV to tens of TeV also arises naturally from the superposition of the two CR components, without the need to invoke non-standard acceleration or propagation effects.

### 3. ASTROPHYSICAL IMPLICATIONS

In this section, we discuss the astrophysical implications of the proposed minimal two-component cosmic-ray framework, focusing on the nature of the source populations that may contribute to the two distinct proton

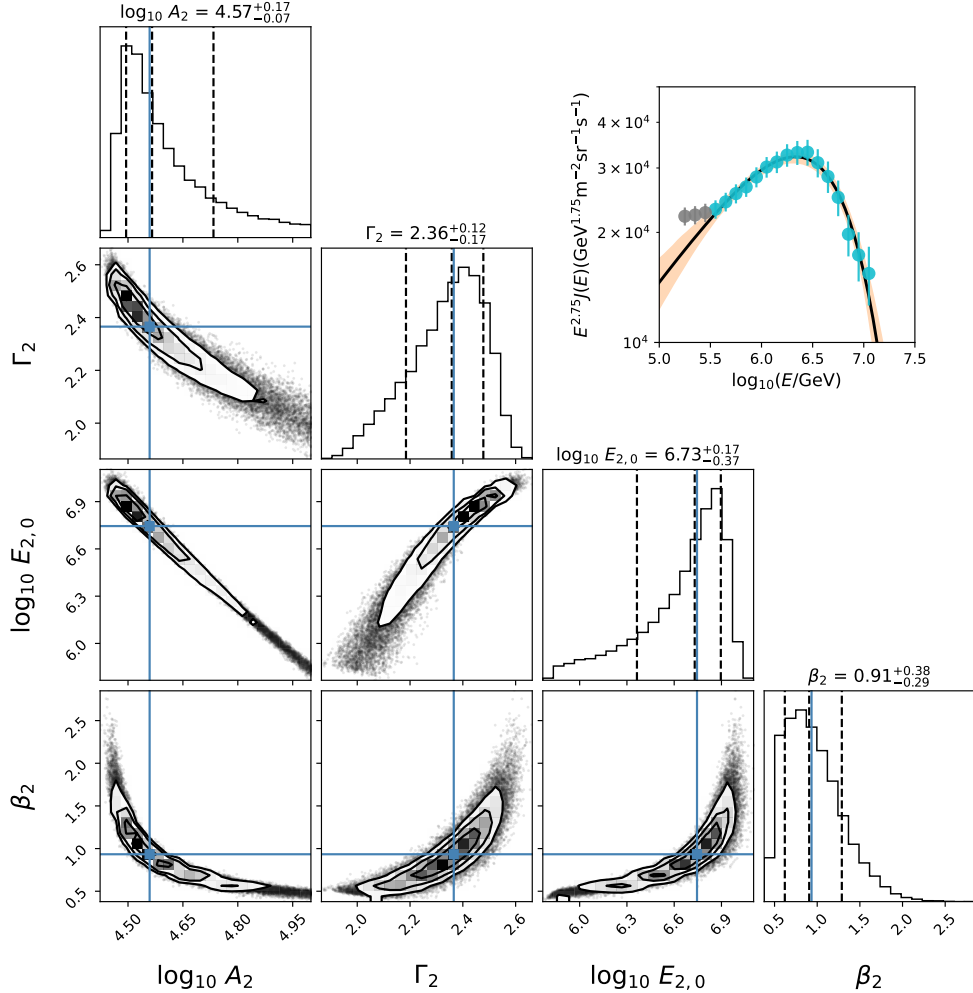


**Figure 3. Main panel:** Corner plot showing the posterior probability distributions for the model parameters for the second component. The sharpness parameter  $\beta_2$  is treated as a free index within the exponential cutoff to characterize the spectral curvature. **Inset:** The observed spectrum compared with the best-fit model (solid black line). The shaded orange region represents the  $1\sigma$  (16th–84th percentile) uncertainty envelope derived from 200 MCMC posterior samples, demonstrating the model’s consistency with the data.

components identified in the spectral analysis. The phenomenological decomposition, by itself, does not allow robust conclusions about individual sources, given the superposition of potential contributions from many objects distributed throughout the Galaxy. Nevertheless, the inferred spectral properties provide meaningful constraints for assessing the plausibility of different classes of Galactic accelerators.

### 3.1. SNR origin of the first CR component

The coherent description of the Galactic CR proton spectrum from GeV to PeV energies within the two-component framework does not require a fundamental revision of the standard SNR paradigm for the origin of Galactic CR. Rather, it supports its validity, albeit within a more limited energy domain extending up to

100 TeV. In this respect, the two-component picture naturally alleviates long-standing tensions associated with the theoretical difficulty of accelerating protons beyond  $\sim 100$  TeV in young SNRs within the standard DSA concept (Lagage & Cesarsky 1983). At the same time, another well-established aspect of this paradigm – the production of relatively hard source spectra and their subsequent steepening due to energy-dependent propagation in the Galactic magnetic fields – remains essentially unchanged.

This interpretation also helps to reconcile the cosmic-ray data with the unexpectedly steep multi-TeV  $\gamma$ -ray spectra observed above  $\sim 1$  TeV from many young SNRs (e.g., Aharonian et al. 2019). These include both classical remnants, such as SN 1006 and Cas A, and more peculiar objects, such as RX J1713.7–3946. However,

caution is required when interpreting these  $\gamma$ -ray observations as direct probes of proton acceleration. Inverse Compton (IC) scattering by relativistic electrons is an efficient radiation mechanism at TeV energies and may dominate over hadronic  $\gamma$ -ray production, particularly in environments where the magnetic field strength does not substantially exceed  $\sim 10 \mu\text{G}$ . As a result, current  $\gamma$ -ray measurements alone do not allow firm conclusions to be drawn regarding the maximum energies attained by accelerated protons.

Moreover, even in the case of a hadronic origin of  $\gamma$ -ray emission, the observed spectral steepening at TeV energies is likely influenced by the escape of the highest-energy particles from the acceleration region, including in relatively young remnants. In this context,  $\gamma$ -ray emission from regions surrounding SNRs may provide a more direct and less biased probe of the maximum proton energies (Aharonian 2013). In the absence of comprehensive morphological studies of young SNRs and their environments, current  $\gamma$ -ray observations alone cannot be regarded as reliable tracers of the maximum proton energies.

The strongest argument in favour of SNRs as the dominant source population responsible for Galactic CRs remains, as for decades, the energetic requirement. The total power available in the form of kinetic energy carried by SNR shocks can reach  $\sim 10^{42} \text{ erg s}^{-1}$ , and it has long been assumed that of order  $\sim 10\%$  of this energy is converted into CRs (Ginzburg & Syrovatskii 1964). This phenomenological estimate is broadly supported by shock acceleration theory (see Malkov & Drury 2001), thus continues to place the SNR population as a major contributor to Galactic CRs.

If the relatively low cutoff energy,  $E_{0,1} \lesssim 100 \text{ TeV}$ , inferred for the first CR proton component is consistent with conservative expectations for the limited potential of DSA operating in the bulk of “standard” SNRs, the super-exponential cutoff required by the data, with  $\beta_1 \gtrsim 2$ , can be interpreted as evidence for a rapid onset of particle escape near the maximum attainable energy. Such behavior may arise from a sudden loss of particle confinement, when the diffusion length of the highest-energy particles becomes comparable to the spatial extent of the acceleration region, enabling efficient upstream escape. One plausible physical mechanism is the breakdown of self-generated magnetic turbulence: above a critical energy, the accelerated particles may no longer sustain the turbulence required for effective confinement, leading to a sharp suppression of the confined proton spectrum. In this regime, insufficient turbulence not only limits the maximum attainable energy to values below  $\sim 100 \text{ TeV}$ , but also naturally produces a very

sharp spectral cutoff. Without entering into the details of this highly complex and model-dependent process, we emphasise that, at a phenomenological level, the data require the first CR component to terminate abruptly, favouring a super-exponential cutoff with  $\beta_1 \gtrsim 2$ .

Another distinct source population – young stellar clusters (YSCs) and, more broadly, star-forming regions – has also long been discussed as a potential contributor to Galactic CRs. Particle acceleration in colliding stellar winds and in the multiple shocks driven by the supernova explosions inside such objects was proposed decades ago as an alternative to isolated SNR (Cesarsky & Montmerle 1983; Bykov 2001). Recent reports of extended diffuse  $\gamma$ -ray emission associated with several stellar clusters, with hard spectra extending up to  $\sim 10 \text{ TeV}$ , have renewed interest in high-energy processes operating in YSCs (Aharonian et al. 2019). This is not unexpected, given that the total mechanical power injected by stellar winds and supernovae in massive clusters is only a factor of a few below the kinetic power released by Galactic supernova explosions, rendering YSCs energetically viable contributors to the Galactic CR budget.

In the proposed two-component framework, YSCs and superbubbles are viewed as complementary acceleration environments rather than primary sources of the first CR population. While their integrated mechanical power may substantially contribute to CR production at lower energies, their defining importance lies in their potential to sustain particle acceleration under extreme and long-lived conditions. This naturally links these systems to the second CR component, which dominates above  $\sim 100 \text{ TeV}$  and requires acceleration sites exceeding the capabilities of the bulk of standard SNRs.

### 3.2. PeVatrons and the second CR component

The detection of dozens of ultra-high-energy (UHE;  $E \gtrsim 100 \text{ TeV}$ )  $\gamma$ -ray sources associated with a variety of astronomical objects (Cao et al. 2024) suggests that the Galaxy hosts a diverse population of PeVatrons rather than a single dominant source class. These objects are natural candidates as sources contributing to the second CR proton component. In the following, we briefly discuss three astrophysical source classes that may contribute to this component. We begin by revisiting the role of supernova remnants, focusing on the possibility that a subset of remnants, under favorable conditions, may operate as PeVatrons. We then consider young stellar clusters and extended star-forming regions as environments where collective effects and clustered supernova activity may enhance particle acceleration to PeV energies. Finally, we discuss microquasars, which were

traditionally underestimated as cosmic-ray accelerators but have recently attracted renewed attention as viable Galactic PeVatron candidates in light of recent UHE  $\gamma$ -ray discoveries.

### 3.2.1. Old SNRs as smoking UHE $\gamma$ -ray guns

While supernova remnants are proposed here as the dominant contributors to the first CR proton component, characterised by a sharp decline above  $\sim 100$  TeV, we cannot exclude the possibility that a subset of SNRs may operate as proton PeVatrons and contribute non-negligibly to the second CR component. Under favourable conditions, acceleration of protons to PeV energies may occur during very early evolutionary stages of SNRs, when shock velocities can reach a significant fraction of the speed of light ( $v_{\text{sh}} \gtrsim 0.03 c$ ) and the magnetic field is strongly amplified, for example through CR-induced instabilities. In these circumstances, the combination of strong shocks, enhanced magnetic turbulence, and high ambient densities can raise the maximum attainable particle energy into the PeV range (e.g. Ptuskin & Zirakashvili 2012; Bell et al. 2013; Blasi 2013).

The absence of UHE  $\gamma$ -ray detections from young SNRs cannot, therefore, be regarded as a decisive argument against their operation as PeVatrons. The short duration of the PeVatron phase and the rapid escape of the highest-energy particles from the remnant make it intrinsically difficult to identify such objects through direct  $\gamma$ -ray observations of young SNR shells.

A more promising approach is provided by indirect searches for so-called “smoking guns”, namely the detection of  $\gamma$ -ray emission produced by CR protons and nuclei that have escaped their accelerator and subsequently interact with nearby giant molecular clouds (GMCs). In this scenario (Aharonian & Atoyan 1996),  $\gamma$ -ray emission may be observed thousands of years after the accelerator itself has faded away.

In the context of supernova remnants, this scenario has long been recognized as a feasible tool for identifying SNRs operating as proton PeVatrons (Gabici & Aharonian 2007). Before being fully diffused and mixed into the Galactic cosmic-ray “sea”, these runaway particles can generate  $\gamma$  rays in nearby massive gas complexes with spectra that differ significantly from those produced in the SNR shell, and that may extend well beyond 100 TeV (Gabici & Aharonian 2007). The realization of this scenario can substantially increase the number of SNR-related systems detectable at ultra-high energies. As suggested in the LHAASO discovery paper (Cao et al. 2021), some of the reported UHE  $\gamma$ -ray sources may indeed be associated with SNR–GMC complexes.

Subsequent dedicated studies aimed at identifying UHE  $\gamma$ -ray emitters from the first LHAASO source catalog (Cao et al. 2024) have indeed revealed several candidate associations with GMCs located near middle-aged SNRs (see, e.g., Mitchell & Celli 2024). The spectra of these sources extend beyond 100 TeV, implying that the energies of the parent particles, most likely protons must reach the PeV scale. While these associations are highly suggestive, they do not yet constitute unambiguous proof of a causal link between UHE  $\gamma$ -ray sources and middle-aged SNRs. Future UHE  $\gamma$ -ray observations with substantially improved angular resolution, combined with comprehensive multiwavelength studies will be essential for establishing whether SNRs can indeed operate as proton PeVatrons.

### 3.2.2. Star-forming regions as sites of proton PeVatrons

Stellar clusters and, more broadly, intensive star-forming regions (SFRs) were identified long ago as efficient CR production sites (e.g., Cesarsky & Montmerle 1983). These regions are characterized by powerful stellar winds from massive stars, which generate enhanced magnetic fields and drive strong turbulence. When combined with strong shocks generated by ongoing supernova activity, these conditions may establish environments more favorable for proton acceleration to PeV energies than those found in isolated SNRs evolving in the average interstellar medium.

Recent  $\gamma$ -ray observations have revealed diffuse UHE  $\gamma$ -ray structures associated with several prominent stellar complexes in the Milky Way, including the most powerful young stellar cluster Westerlund 1 (Aharonian et al. 2022), the giant Cygnus Cocoon (Cao et al. 2022), and one of the most active Galactic star-forming regions, W43 (Cao et al. 2025). Of particular interest is the Cygnus Cocoon, whose  $\gamma$ -ray spectrum extends into the PeV range (Cao et al. 2022), implying the presence of PeV protons. An interpretation of the UHE  $\gamma$ -ray emission in terms of inverse Compton scattering by electrons is strongly disfavored, given the rapid synchrotron losses that prevent electrons from reaching PeV energies in typical magnetic-field environments.

Particle acceleration within stellar clusters may proceed through two major scenarios. The first involves direct acceleration at shocks generated by colliding stellar winds, which can efficiently accelerate particles to multi-TeV energies. However, detailed theoretical studies indicate that achieving the PeV domain through stellar-wind interactions alone is highly challenging (e.g., Morlino et al. 2019; Vieu et al. 2022; Härer et al. 2025).

Alternatively, supernovae occurring within stellar clusters may play a more decisive role. In this scenario,

supernova shocks propagate into a pre-existing, highly turbulent and strongly magnetized medium created by stellar winds, which can significantly enhance acceleration efficiency and relax constraints on the maximum attainable particle energy (Vieu et al. 2022). This process is particularly relevant for the loose stellar association Cygnus OB2 in the Cygnus region. In this case, the stellar association itself does not act as the PeV proton accelerator; rather, it establishes favorable physical conditions that enable a powerful supernova, possibly one that exploded several  $\times 10^4$  years ago, to accelerate protons up to PeV energies, potentially accounting for the UHE  $\gamma$ -ray emission detected toward the Cygnus region (Härer et al. 2025).

Nevertheless, even under the most favorable conditions, explaining the extension of the Cygnus Cocoon spectrum to PeV energies remains challenging, suggesting that additional or alternative, exceptionally powerful PeVatron candidates may contribute to the observed PeV  $\gamma$ -ray emission.

### 3.2.3. Microquasars as potential PeVatrons

Microquasars are luminous X-ray binaries hosting a stellar-mass black hole or neutron star that launch collimated, accretion-powered outflows. The kinetic power of these jets can episodically reach  $L_K \simeq 10^{38} - 10^{40}$  erg s $^{-1}$ , comparable to, or even exceeding, the Eddington luminosity of the compact object. Such extreme power output establishes favorable conditions for transient PeVatron activity (Peretti et al. 2025; Wang et al. 2025; Kaci et al. 2025).

Within the framework of ideal magnetohydrodynamics, the maximum energy attainable by a proton is constrained by the electric potential drop across the system and can be estimated as (Wang et al. 2025)

$$E_{\max} \approx 10 \left( \frac{L_K}{10^{38} \text{ erg s}^{-1}} \right)^{1/2} \left( \frac{\sigma v}{c} \right)^{1/2} \text{ PeV}, \quad (3)$$

where  $v$  denotes the jet velocity,  $c$  is the speed of light, and  $\sigma$  is the magnetization parameter characterizing the fraction of kinetic energy converted into Poynting flux. Thus, microquasars in high-accretion states, with relativistic jets of mechanical power  $L_K \gtrsim 10^{39}$  erg s $^{-1}$  and moderate magnetization ( $\sigma \gtrsim 0.1$ ), can in principle accelerate protons to energies exceeding  $\sim 10$  PeV.

Recent detections of diffuse UHE  $\gamma$ -ray emission in the vicinity of several powerful Galactic microquasars (Alfaro et al. 2024a; H.E.S.S. Collaboration 2024; Alfaro et al. 2024b; H.E.S.S. Collaboration 2025; LHAASO Collaboration 2025a) place microquasars firmly within the growing class of Galactic PeVatron candidates. In the case of the most powerful system in the Galaxy, SS 433,

the multi-TeV emission exhibits a pronounced energy-dependent morphology (H.E.S.S. Collaboration 2024), which is most naturally explained by inverse Compton scattering of relativistic electrons.

Meanwhile, the detection by LHAASO of UHE  $\gamma$  rays extending beyond 100 TeV (LHAASO Collaboration 2025a) indicates the presence of an additional high-energy emission component that is difficult to reconcile with a purely leptonic origin and more naturally points to hadronic processes. Even more compelling is the detection of  $\gamma$  rays with energies well above 100 TeV from V4641 Sgr (LHAASO Collaboration 2025a), which is extremely difficult to accommodate within any reasonable inverse Compton framework.

Finally, the most compelling evidence for proton acceleration to PeV energies is provided by the discovery of PeV  $\gamma$  rays from the microquasar Cygnus X-3 by the LHAASO collaboration (LHAASO Collaboration 2025b). The observed flux variability and its modulation with the 4.8 h orbital period demonstrate that the parent particles are accelerated within the extremely compact binary system itself, leaving little room for an interpretation of the  $\gamma$ -ray emission in terms of leptonic processes. The modulated signal, characterised by an unusually hard spectrum extending up to  $\sim 3$  PeV, is most naturally explained by photomeson production resulting from interactions of protons with energies exceeding  $\sim 10$  PeV with the intense optical/UV radiation field of the massive companion star (LHAASO Collaboration 2025b). This discovery can therefore be regarded as the first unambiguous identification of a Galactic proton PeVatron.

From a theoretical standpoint, microquasars offer two plausible sites for proton acceleration to extreme energies. The first involves internal shocks within the compact, relativistic jets formed inside the binary system, as inferred in the case of Cygnus X-3. The second corresponds to jet-termination shocks developing at distances of tens of parsecs from the source, as suggested for V4641 Sgr and possibly also for Cygnus X-3, if the extended UHE  $\gamma$ -ray emission observed toward the Cygnus region originates from a halo powered by the microquasar outflow<sup>2</sup>. The substantial kinetic power transported by relativistic jets renders microquasars natural candidates for both persistent and transient PeVatron activity.

<sup>2</sup> This interpretation, as an alternative to a link with the Cygnus OB2 stellar association, cannot be excluded *a priori*. Moreover, it alleviates the theoretical tension associated with accelerating multi-PeV protons in this powerful but loosely bound stellar association.

The energy necessary to sustain the observed PeV CR proton flux  $\dot{W}_{\text{CR}}(\geq 1 \text{ PeV})$  is estimated between  $\sim 10^{38}$  to  $10^{39} \text{ erg s}^{-1}$ , depending on the highly uncertain confinement time of PeV protons inside the Galaxy. This implies that even a single or a small number of powerful microquasars could, in principle, supply the PeV CR flux, given that the acceleration of protons to PeV energies requires a comparable amount of power in individual sources. Indeed, it has been shown that the presence of only  $\sim 10$  active powerful microquasars in the Galaxy at any given time is sufficient to reproduce CR and  $\gamma$ -ray data within a self-consistent framework (Kaci et al. 2025). At the same time, the total power released by the microquasar population remains well below the injection rate required to sustain the overall Galactic CR luminosity,  $\dot{W}_{\text{CR,tot}} \simeq 10^{41} \text{ erg s}^{-1}$ . Consequently, in our two-component cosmic-ray proton framework, microquasars cannot provide a significant contribution to the low-energy component, in a good agreement with Fig.1.

The extension of the CR proton spectrum beyond 10 PeV (see Fig.2) raises an important question as to whether microquasars could also be responsible for this component of the spectrum, at least up to 100 PeV. The answer is straightforward; as it follows from Eq. (3), achieving these energies would require jet powers that are unrealistically large, exceeding  $\sim 10^{40} \text{ erg s}^{-1}$ .

Thus, if the component of CR protons extending well beyond 10 PeV is of Galactic origin, individual objects or phenomena more powerful than microquasars and supernova explosions are required. In this context, the supermassive black hole at the Galactic Center, Sgr A\*, appears to be the only viable candidate within the Milky Way. Although Sgr A\* currently accretes at a very low rate, corresponding to  $\sim 10^{-8} L_{\text{Edd}}$  for a black hole of mass of  $\sim 4 \times 10^6 M_{\odot}$ , its activity in the past may have been orders of magnitude higher. During such active phases, Sgr A\* could in principle satisfy the conditions required for the acceleration of protons to energies approaching, or even exceeding, 100 PeV. Interestingly, Sgr A\* has been proposed as a Galactic PeVatron injecting protons into the Central Molecular Zone in order to explain the diffuse multi-TeV  $\gamma$ -ray emission observed from that region (HESS Collaboration 2016). However, this hypothesis requires confirmation through  $\gamma$ -ray observations extending into the PeV energy range.

#### 4. SUMMARY

Recent high-precision measurements of the CR proton spectrum reveal clear deviations from a simple power-law behaviour, including (i) progressive spectral hardening above  $\sim 200 \text{ GeV}$ , (ii) a pronounced excess in the 10–30 TeV range followed by a sharp turnover around  $\sim 100 \text{ TeV}$ , and (iii) a broad spectral structure extending from  $\sim 0.1$  to several PeV. These features cannot be readily explained within a single-component framework based solely on standard acceleration and propagation effects.

In this work, we have shown that the entire proton spectrum from GeV to PeV energies can be consistently described by the superposition of two broad Galactic CR proton populations. In this minimal two-component framework, the observed spectral complexity arises naturally from the transition between a low-energy component with a sharp cutoff at tens of TeV and a second, harder component that dominates above  $\sim 100 \text{ TeV}$  and extends to PeV energies.

The suggested model reproduces all major spectral features without invoking highly contrived acceleration or propagation scenarios. Moreover, the present data do not require a dominant contribution from a nearby or local source to explain the observed proton spectrum. While such sources cannot be excluded in principle, the two-component interpretation provides a population-based explanation at the Galactic scale, and is therefore favoured on grounds of simplicity. In this sense, the proposed model follows the spirit of Occam's razor, introducing no additional ingredients beyond those minimally required by the data.

Finally, although our analysis focuses on protons, the two-component framework has important implications for heavier CR nuclei. If the relative contributions or elemental compositions of the two components differ, distinct spectral features may emerge for different species, particularly in the energy range where the components overlap. Precision measurements of individual nuclear spectra and composition in the multi-TeV to sub-PeV range will therefore provide a critical and independent test of the two-component scenario.

<sup>1</sup> B.T.Z. is supported in China by the National Key R&D program of China under the grant 2024YFA1611402.

#### REFERENCES

Adriani, O., Akaike, Y., Asano, K., et al. 2022, *PhRvL*, 129, 101102, doi: [10.1103/PhysRevLett.129.101102](https://doi.org/10.1103/PhysRevLett.129.101102)

Aguilar, M., et al. 2015, *Phys. Rev. Lett.*, 114, 171103, doi: [10.1103/PhysRevLett.114.171103](https://doi.org/10.1103/PhysRevLett.114.171103)

Aharonian, F., Ashkar, H., & Backes, M., e. 2022, *A&A*, 666, A124, doi: [10.1051/0004-6361/202244323](https://doi.org/10.1051/0004-6361/202244323)

Aharonian, F., Yang, R.-Z., & de Oña Wilhelmi, E. 2019, *Nature Astronomy*, 3, 561, doi: [10.1038/s41550-019-0724-0](https://doi.org/10.1038/s41550-019-0724-0)

Aharonian, F. A. 2013, *Astroparticle Physics*, 43, 71, doi: [10.1016/j.astropartphys.2012.04.004](https://doi.org/10.1016/j.astropartphys.2012.04.004)

Aharonian, F. A., & Atoyan, A. M. 1996, *A&A*, 309, 917

Ahn, H. S., Allison, P., Bagliesi, M. G., et al. 2010, *ApJL*, 714, L89, doi: [10.1088/2041-8205/714/1/L89](https://doi.org/10.1088/2041-8205/714/1/L89)

Alemanno, F., et al. 2025a, <https://arxiv.org/abs/2511.05409>

—. 2025b, <https://arxiv.org/abs/2511.05409>

Alfaro, R., Alvarez, C., Arteaga-Velázquez, J. C., et al. 2024a, *Astrophysical Journal*, 976, 30, doi: [10.3847/1538-4357/ad7e1b](https://doi.org/10.3847/1538-4357/ad7e1b)

—. 2024b, *Nature*, 634, 557, doi: [10.1038/s41586-024-07995-9](https://doi.org/10.1038/s41586-024-07995-9)

Antoni, T., Apel, W., Badea, A., et al. 2005, *Astroparticle Physics*, 24, 1, doi: <https://doi.org/10.1016/j.astropartphys.2005.04.001>

Atkin, E., et al. 2017, *JCAP*, 07, 020, doi: [10.1088/1475-7516/2017/07/020](https://doi.org/10.1088/1475-7516/2017/07/020)

Bell, A. R. 2004, *Monthly Notices of the Royal Astronomical Society*, 353, 550

Bell, A. R., Schure, K. M., Reville, B., & Giacinti, G. 2013, *Monthly Notices of the Royal Astronomical Society*, 431, 415, doi: [10.1093/mnras/stt179](https://doi.org/10.1093/mnras/stt179)

Berezinskii, V. S., Bulanov, S. V., Dogiel, V. A., Ginzburg, V. L., & Ptuskin, V. S. 1990, *Astrophysics of Cosmic Rays* (North-Holland)

Blandford, R., & Eichler, D. 1987, *Phys. Rep.*, 154, 1, doi: [10.1016/0370-1573\(87\)90056-4](https://doi.org/10.1016/0370-1573(87)90056-4)

Blasi, P. 2013, *Astron. Astrophys. Rev.*, 21, 70, doi: [10.1007/s00159-013-0070-7](https://doi.org/10.1007/s00159-013-0070-7)

Blasi, P., Amato, E., & Serpico, P. D. 2012, *PhRvL*, 109, 061101, doi: [10.1103/PhysRevLett.109.061101](https://doi.org/10.1103/PhysRevLett.109.061101)

Bykov, A. M. 2001, *SSRv*, 99, 317, doi: [10.1023/A:1013817721725](https://doi.org/10.1023/A:1013817721725)

Cao, Z., Aharonian, F., , & Axikegu, Y. e. 2022, *Chinese Physics C*, 46, 035001, doi: [10.1088/1674-1137/ac3fa4](https://doi.org/10.1088/1674-1137/ac3fa4)

Cao, Z., Aharonian, F., & An, Q., e. 2024, *ApJS*, 271, 25, doi: [10.3847/1538-4365/acfd29](https://doi.org/10.3847/1538-4365/acfd29)

Cao, Z., Aharonian, F., & Axikegu Y.X., e. 2025, *Science China Physics, Mechanics, and Astronomy*, 68, 279502, doi: [10.1007/s11433-024-2477-9](https://doi.org/10.1007/s11433-024-2477-9)

Cao, Z., Aharonian, F. A., & An, Q., e. 2021, *Nature*, 594, 33, doi: [10.1038/s41586-021-03498-z](https://doi.org/10.1038/s41586-021-03498-z)

Cao, Z., et al. 2025, *Sci. Bull.*, 70, 4173, doi: [10.1016/j.scib.2025.10.048](https://doi.org/10.1016/j.scib.2025.10.048)

Cesarsky, C. J., & Montmerle, T. 1983, *SSRv*, 36, 173, doi: [10.1007/BF00167503](https://doi.org/10.1007/BF00167503)

Gabici, S., & Aharonian, F. A. 2007, *ApJL*, 665, L131, doi: [10.1086/521047](https://doi.org/10.1086/521047)

Gabici, S., Evoli, C., Gaggero, D., et al. 2019, *Int. J. Mod. Phys. D*, 28, 1930022, doi: [10.1142/S0218271819300222](https://doi.org/10.1142/S0218271819300222)

Ginzburg, V. L., & Syrovatskii, S. I. 1964, *The Origin of Cosmic Rays* (Pergamon Press)

Grenier, I. A., Black, J. H., & Strong, A. W. 2015, *Annu. Rev. Astron. Astrophys.*, 53, 199, doi: [10.1146/annurev-astro-082214-122457](https://doi.org/10.1146/annurev-astro-082214-122457)

Härer, L., Vieu, T., Schulze, F., Larkin, C. J. K., & Reville, B. 2025, *A&A*, 703, A111, doi: [10.1051/0004-6361/202555531](https://doi.org/10.1051/0004-6361/202555531)

HESS Collaboration. 2016, *Nature*, 531, 476, doi: [10.1038/nature17147](https://doi.org/10.1038/nature17147)

H.E.S.S. Collaboration. 2024, *Science*, 383, 402, doi: [10.1126/science.adi2048](https://doi.org/10.1126/science.adi2048)

—. 2025, *Astronomy & Astrophysics*, <https://arxiv.org/abs/arXiv:2511.10537>

Hörandel, J. R. 2003, *Astroparticle Physics*, 19, 193

Kaci, S., Giacinti, G., Aharonian, F., & Wang, J.-S. 2025, arXiv e-prints, arXiv:2510.01369, doi: [10.48550/arXiv.2510.01369](https://doi.org/10.48550/arXiv.2510.01369)

Kulikov, G. V., & Khristiansen, G. B. 1959, *Sov. Phys. JETP*, 8, 441

Lagage, P. O., & Cesarsky, C. J. 1983, *Astronomy and Astrophysics*, 118, 223

LHAASO Collaboration. 2025a, *National Science Review*, 12, nwaf496, doi: [10.1093/nsr/nwaf496](https://doi.org/10.1093/nsr/nwaf496)

—. 2025b, arXiv e-prints, <https://arxiv.org/abs/arXiv:2512.16638>

Liu, W., Guo, Y.-Q., & Yuan, Q. 2019, *JCAP*, 10, 010, doi: [10.1088/1475-7516/2019/10/010](https://doi.org/10.1088/1475-7516/2019/10/010)

Malkov, M. A., & Drury, L. O. 2001, *Rep. Prog. Phys.*, 64, 429, doi: [10.1088/0034-4885/64/4/201](https://doi.org/10.1088/0034-4885/64/4/201)

Malkov, M. A., & Moskalenko, I. V. 2021, *ApJ*, 911, 151, doi: [10.3847/1538-4357/abe855](https://doi.org/10.3847/1538-4357/abe855)

Mitchell, A. M. W., & Celli, S. 2024, *Journal of High Energy Astrophysics*, 44, 340, doi: [10.1016/j.jheap.2024.10.011](https://doi.org/10.1016/j.jheap.2024.10.011)

Morlino, G., Blasi, P., & Peretti, E. 2019, *Monthly Notices of the Royal Astronomical Society*, 487, 4547

Peretti, E., Petropoulou, M., Vasilopoulos, G., & Gabici, S. 2025, *A&A*, 698, A188, doi: [10.1051/0004-6361/202452987](https://doi.org/10.1051/0004-6361/202452987)

Ptuskin, V., & Zirakashvili, V. 2012, *Astronomy & Astrophysics*, 543, A47,  
doi: [10.1051/0004-6361/201118643](https://doi.org/10.1051/0004-6361/201118643)

Strong, A. W., Moskalenko, I. V., & Ptuskin, V. S. 2007,  
*Annu. Rev. Nucl. Part. Sci.*, 57, 285,  
doi: [10.1146/annurev.nucl.57.090506.123011](https://doi.org/10.1146/annurev.nucl.57.090506.123011)

Varsi, F., Ahmad, S., Chakraborty, M., et al. 2024, *PhRvL*,  
132, 051002, doi: [10.1103/PhysRevLett.132.051002](https://doi.org/10.1103/PhysRevLett.132.051002)  
Vieu, T., Reville, B., & Aharonian, F. 2022, *Monthly Notices of the Royal Astronomical Society*, 515, 5600,  
doi: [10.1093/mnras/stac2134](https://doi.org/10.1093/mnras/stac2134)  
Wang, J., Reville, B., & Aharonian, F. A. 2025, *ApJL*, 989,  
L25, doi: [10.3847/2041-8213/adf3a4](https://doi.org/10.3847/2041-8213/adf3a4)